



Original paper

## Statistical and spatial correlation between diffusion and perfusion MR imaging parameters: A study on soft tissue sarcomas



Georgios S. Ioannidis<sup>a,b,\*</sup>, Katerina Nikiforaki<sup>a,b</sup>, Apostolos Karantanas<sup>a,b,c</sup>

<sup>a</sup> Foundation for Research and Technology – Hellas (FORTH), Institute of Computer Science (ICS), Computational Bio-Medicine Laboratory (CBML), Heraklion, Greece

<sup>b</sup> Medical School, University of Crete, Heraklion, Greece

<sup>c</sup> Department of Medical Imaging, University Hospital, Heraklion, Greece

## ARTICLE INFO

## Keywords:

Dynamic contrast enhanced MR imaging  
Diffusion Weighted Imaging  
Musculoskeletal tumors  
Soft tissue sarcoma  
Intravoxel incoherent motion

## ABSTRACT

**Purpose:** The purpose of this study was to examine the correlation of diffusion and perfusion quantitative MR parameters, on patients with malignant soft tissue tumors. In addition, we investigated the spatial agreement of hallmarks of malignancy as indicated by diffusion and perfusion biomarkers respectively.

**Methods:** Nonlinear least squares were used for the quantification of the DWI and DCE derived parameters for 25 patients of histologically proven soft tissue sarcoma scanned at a 1.5 T scanner. 4D data were analyzed by an in house built software implemented in Python 3.5 resulting in voxel based parametric maps based on the Intra-Voxel Incoherent Motion (IVIM), Extended Toft's (ETM) and Gamma Capillary Transit time (GCTT) models. The root mean squared error (RMSE) was also used for assessing the accuracy of the DCE fitting models.

**Results:** A good Pearson's correlation ( $r > 0.5$ ) was found between micro-perfusion fraction (f-IVIM) and plasma volume (vp-GCTT). There was no significant correlation between all other possible pairs of DCE and DWI derived parameters. Following thresholding the indicators of malignancy from both imaging methods, the percentage of volume overlap between regions of high cellularity and high vascular permeability ranged from 6% to 30%.

**Conclusion:** A free correlation study among all DCE and DWI derived pairs of parameters, showed a linear relationship between f-IVIM and vp-GCTT in patients with soft tissue sarcomas. DCE in conjunction with DWI MRI can provide useful information on sites of aggressive characteristics for guiding the pre-operative biopsy and for overall treatment planning.

### 1. Introduction

Dynamic contrast enhanced magnetic resonance imaging (DCE-MRI) is one of the most commonly used imaging techniques for capturing the perfusion characteristics of biological tissues. DCE-MRI acquisition studies include vascular permeability, tissue perfusion, and expansions of extravascular-extracellular spaces (EES) based on a series of T1-weighted (T1W) images, acquired before, during and after intra venous injection of gadolinium based contrast agent [1]. A number of mathematical models under certain assumptions can be fitted to the DCE signal intensity time curves to extract perfusion relevant biomarkers.

Diffusion Weighted Imaging (DWI) contrast stems from two distinct physiological mechanisms and thus highlights more than one process. The first mechanism of diffusion contrast is the restriction of water

movement in the intra- and extra- cellular space (molecular diffusion or Brownian motion) [2]. The second one, is related to the blood micro-circulation in the randomly distributed micro-capillary network [3]. The degree of diffusion weighting (DW) is tailored by the b-value parameter (in  $s/mm^2$ ) which is related to the amplitude and time of the diffusion sensitizing gradients of the sequence. When ignoring the contribution of microcirculation in the signal, DW is considered to follow a mono-exponential decay as a function of b, resulting in Apparent Diffusion Coefficient (ADC) ( $mm^2/s$ ). However, when studying complex systems like tissue, both concurrent phenomena of diffusion and perfusion have to be taken into account. Le Bihan et al. suggested the Intra-Voxel Incoherent Motion (IVIM) model resulting in a set of 3 parameters describing cellular density (D), vascular portion of the voxel (f) and the pseudo diffusion coefficient  $D^*$ . Taking into account that DWI does not require the administration of contrast medium, the study

\* Corresponding author at: Computational Bio-Medicine Laboratory, Foundation for Research and Technology – Hellas, 100 Nikolaou Plastira Str., Vassilika Vouton, P.O. Box 1385, Heraklion, Crete GR 700 13, Greece.

E-mail address: [grs.ioannidis@gmail.com](mailto:grs.ioannidis@gmail.com) (G.S. Ioannidis).

URL: <http://www.ics.forth.gr/cbml/> (G.S. Ioannidis).

<https://doi.org/10.1016/j.ejmp.2019.08.007>

Received 8 May 2019; Received in revised form 18 July 2019; Accepted 5 August 2019

Available online 13 August 2019

1120-1797/© 2019 Associazione Italiana di Fisica Medica. Published by Elsevier Ltd. This is an open access article under the CC BY-NC-ND license (<http://creativecommons.org/licenses/by-nc-nd/4.0/>).

of tissue vascularity alongside cellularity with a single readily available sequence is of utmost importance. Henceforth, a study of correlation between perfusion parameters derived from DWI and DCE-MRI is an open field of research in the broad field of oncology. Positive correlation of perfusion related parameters between DCE-MRI and DWI has been shown in the literature for different sites of the human body [4–7].

Soft tissue tumors compose a very heterogeneous group of neoplasms requiring different therapeutic management [4]. However they often exhibit overlapping imaging characteristics and thus assessment based on conventional radiological features can be challenging. Quantitative biomarkers derived from an extended MRI protocol can non-invasively offer an insight into tissue architecture and support an accurate diagnosis. Preoperative biopsy aims at targeting the most aggressive part of the tumor in order to assess parameters including cell type, cellular atypia, number of mitoses and presence of necrosis and conclude on tumor type preoperatively. However, tumor heterogeneity and large lesion size hinder correct and accurate tumor sampling. To this end, radiological guidance of biopsy based on advanced MRI biomarkers can be a valuable tool for well targeted biopsy and efficient therapeutic management.

The present study examines the possible correlation of DWI and DCE imaging markers, indicative of cellularity and vascularity respectively, derived from well-established mathematical models (IVIM for DWI while ETM and GCTT for DCE as described in the following sections). In addition, fitting performance of each perfusion model is evaluated in terms of the root mean squared error (RMSE). As both vascularity and cellularity are measures of tumor aggressiveness, we studied the spatial correlation of relevant imaging markers in order to have a visual representation of the most malignant parts. The possible benefit of DWI and DCE positive correlation is related to the simplification of the MRI protocol without significant loss of information. The impact of spatial correlation of DWI and DCE metrics of malignancy is the mitigation of possible sampling errors from pre-operative biopsy, which might underestimate the tumor grade or even give a false negative result.

## 2. Materials and methods

### 2.1. Workflow

In our University Hospital, patients with a suspicious soft tissue mass, undergo MRI examination with a specific oncologic MR protocol before any biopsy. Following MRI, biopsy, either with CT or US guidance is planned and depending upon the results, the patients are planned for surgical excision. The removed tumor is immediately transferred to histopathologic department for analysis. Imaging and histopathologic data are collected for further post processing. The above described workflow is graphically presented in Fig. 1. Each step of this process is described in detail in the following sections.

### 3. Patient population

30 patients (18 males, 12 females median age: 63 y) with suspicion for soft tissue tumor (STT) underwent MRI examination during a 2 year study period (2016–2018). Exclusion criteria apart from contraindications to MRI (pacemakers, ferromagnetic implants, claustrophobia, contraindications for administration of Gadolinium contrast medium), were STT showing no enhancement or no abnormal signal on fat suppressed DWI such as well differentiated liposarcomas (3) or benign lipomas (2). Moreover, severe image degradation from artifacts especially for abdominal STT also led to the exclusion of 3 patients. The examination protocol has been approved by the local ethics committee and all patients have signed an informed consent for the use of their data for research purposes. The patient cohort of the analysis comprised the following STT: 6 dedifferentiated liposarcoma, 5 pleomorphic liposarcoma, 4 myxoid liposarcoma, 4 leiomyosarcoma, 2 alveolar sarcoma, 3 malignant peripheral nerve sheath sarcoma, 1 Ewing sarcoma.

## 4. MRI protocol

Each of 25 patients underwent MR examination on a 1.5 T clinical MR scanner (Vision/Sonata Hybrid system, Siemens, Erlangen, Germany) equipped with powerful gradients (Strength: 45 mT/m, Slew rate: 200 mT/m/ms). The imaging protocol, apart from the conventional sequences, included DWI and DCE-MRI quantitative techniques. Depending on the lesion site the appropriate choice of coil and FOV was made on the basis of complete lesion coverage at highest SNR. DW axial images were acquired utilizing an EPI (Echo Planar Imaging) sequence with fat suppression, diffusion sensitizing gradients in 3 directions ( $b = 0, 50, 100, 150, 200, 500, 800, 1500 \text{ s/mm}^2$ ), number of slices = 14–18, echo time (TE) = 100 ms, repetition time (TR) = 3500 ms, matrix size =  $128 \times 128$ , field of view either (FOV) =  $200 \times 200 \text{ mm}$  (alternative for torso  $400 \times 400 \text{ mm}$ ), slice thickness = 5 mm. This technique has been applied for the reduction of machine related geometrical distortions or apparent distortions in signal intensities. T1W DCE perfusion MR imaging was performed by utilizing a 3D VIBE (volume interpolated breath hold examination) sequence in the axial plane with variable flip angles (FA = 5°, 10°, 15°, 20°, 25°, 30°) for the initial calculation of the parametric T1 maps. Consequently, an intravenous bolus injection of the paramagnetic CA (Magnevist, Gadopentetate Dimeglumine, Bayer Healthcare, Bayer, 0.1 mmol/kg) was performed. The aforementioned T1W DCE VIBE perfusion sequence comprised 45 dynamic acquisitions (6.5 s temporal resolution) after the intravenous injection of the CA with the following imaging parameters: number of slices = 14, FA = 15°, TE = 3.23 ms, TR = 7.1 ms, matrix size =  $384 \times 384$ , FOV =  $200 \times 200 \text{ mm}$  ( $400 \times 400 \text{ mm}$ ) and slice thickness = 5 mm.

## 5. Histopathologic analysis

Within a period of 14 days after MR examination, all patients underwent surgery during which the surgeon marked the specimen with sutures in predefined points in order to enable the actual three-dimensional orientation of the specimen in relation with the patient's body. The excised specimens were transferred to the department of pathology for classification and grading. The outer surface of the specimen was marked with permanent ink in order to identify the surgical markings. The pathologist confirmed the original orientation of the specimen in the body based on the sutures and then cut consecutive thin slices from the top and the bottom of the specimen in order to identify the upper and lower rim of the neoplasm. The central slice of the tumor, corresponding to the lesion's central imaging slice, was selected after measuring the distances from the upper and lower margins, was divided in orthogonal slabs (in a grid-manner), and placed into plastic cassettes (Fig. 1(b)). Tumor tissue sections were processed according to CAP guidelines [5] and recommendations for specimen handling 4  $\mu\text{m}$  thick sections of each tumor slab were cut, placed into glass slides, stained and examined microscopically (Nikon Eclipse E-200) in order to characterize each area of the central tumor slice in terms of differentiation, cell type, cellular atypia, cellularity, mitotic activity, vascularity and presence of necrosis. More specifically, Ki-67 staining, indicative of mitotic activity was used to give insight into the presence of areas of high or low cellularity which is also the contrast mechanism of DWI. Analogously, CD 34 staining, indicative of vascular density was performed to locate highly perfused areas of the tumor to be studied alongside with DCE imaging Fig. 1(c). Histopathologic analysis results were used to verify findings from MRI data post processing analysis, graphically represented as voxel-based parametric maps and ROI histograms in order to have a visual overview of the distribution of the calculated values for each marker Fig. 1(d).

**IVIM-MRI analysis** The quantification of diffusion and perfusion parameters was implemented in python 3.5 (www.python.org). The parametric maps were extracted with the trust region reflective algorithm, of the SciPy library (scipy.optimize.least\_squares).

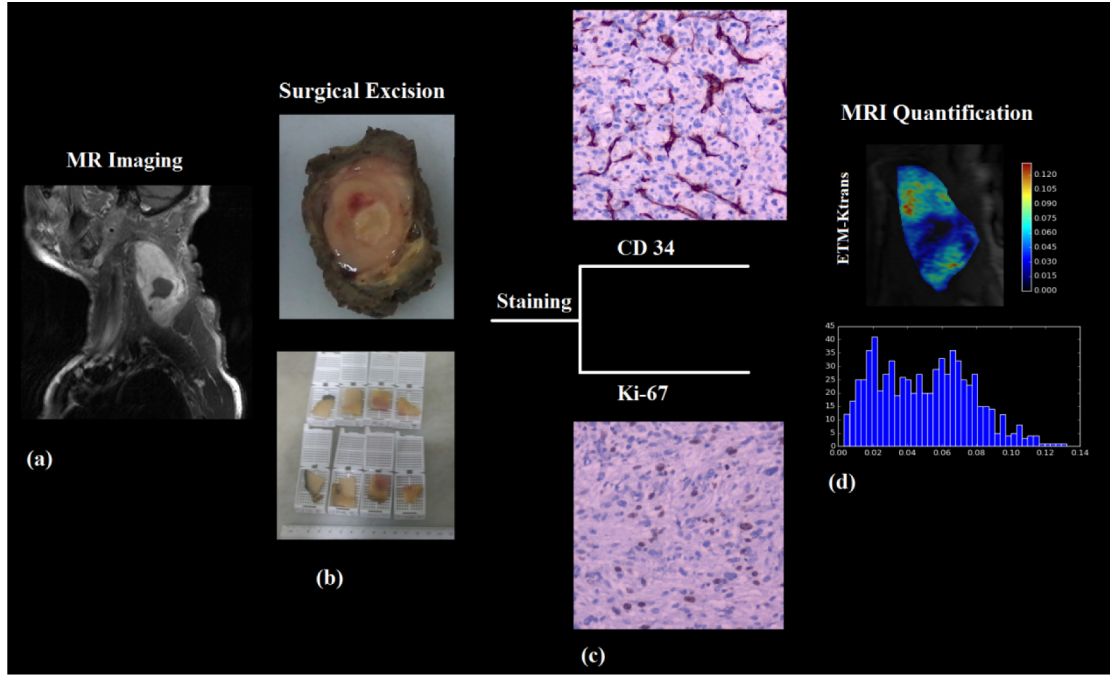


**Fig. 1.** Workflow description. (a) MR imaging (fat suppressed contrast enhanced T1W) of a soft tissue mass in the neck. (b) Surgically excised specimen and tissue preparation sampling for staining. (c) Assessment of vascularity (CD 34) and mitotic activity (Ki-67) based on specific staining. (d) Quantitative analysis of MR data, indicative Ktrans parametric map and the corresponding histogram.

The DWI signal of a homogeneous medium, has a dominant mono-exponential decay curve of the form:  $S(b)/S(0) = e^{-bADC}$  [6]. Apparent diffusion coefficient (ADC) represents the mean displacement of water molecules (typically a random walk) in space [2]. Le Bihan et al. proposed that micro-perfusion in the capillary network contributes to the DWI signal decay as a random walk (pseudo-random) because of the arbitrary organization of the capillary network [3]. Thus, perfusion information can be obtained by the intra-voxel incoherent motion (IVIM) model as:

$$S(b)/S(0) = (1 - f)e^{-bD} + fe^{-bD^*} \quad (1)$$

where,  $S(b)$  is the measured signal intensity at the current b-value and  $S(0)$  is the measured signal intensity with  $b = 0$ , meaning no diffusion weighting,  $D$  is the diffusion coefficient,  $D^*$  is the pseudo-diffusion coefficient which is considered as an order of magnitude greater than  $D$  and  $f$  is the micro-perfusion fraction that reflects the ratio of water flowing in capillaries to the total water contained in a voxel.

The IVIM parameters were obtained by using the aforementioned nonlinear fitting algorithm with the following constraints for each parameter:

$$f \in [0, 1], D \in [0, 5] \times 10^{-3} \text{mm}^2/\text{s}, D^* \in [10, 200] \times 10^{-3} \text{mm}^2/\text{s}.$$

## 6. DCE-MRI analysis

The conversion of the MR signal to concentration of the contrast agent (CA) in the tissues  $C_t(t)$  was performed utilizing the flip angle method [7]. For the quantification of the DCE-MRI signal, two pharmacokinetic models from the bibliography were selected. The first is the widely known Extended Tofts model (ETM) [8] with three parameters ( $K_{trans}$ ,  $K_{ep}$ ,  $v_p$ ) as shown in Eq. (2).

$$C_t(t) = K_{trans} e^{-K_{ep}t} \otimes C_a(t) + v_p C_a(t) \quad (2)$$

The symbol  $\otimes$  represents the convolution operator,  $K_{trans} \text{min}^{-1}$  is the transfer constant from the blood plasma into the EES and  $K_{ep} \text{min}^{-1}$  is the transfer constant from the EES back to the blood plasma while  $v_p$  stands for the plasma volume and  $C_a(t)$  for the time concentration curve of a feeding artery, also known as the arterial input function (AIF).

The second model used in our analysis is the Gamma capillary transit time model (GCTT) [9] described by Eq. (3).

$$C_t(t) = F \left[ \gamma \left( \frac{1}{a^{-1}}, \frac{t}{\tau} \right) + \frac{E e^{-K_{ep}t}}{(1 - K_{ep}\tau)^{1/a^{-1}}} \left[ 1 - \gamma \left( \frac{1}{a^{-1}}, \left( \frac{1}{\tau} - K_{ep} \right) t \right) \right] \right] \otimes C_a(t) \quad (3)$$

The recently suggested GCTT model, unifies four well-known models such as the Tofts Model [8], the ETM, the adiabatic tissue homogeneity (ATH) model [10] and the two compartment exchange (2CX) model [11] depending on the value of  $a^{-1}$  being the shape parameter of the Gamma distribution of the capillary transit times.  $F \text{ mL/mL/min}^{-1}$  is the blood flow or blood perfusion,  $a^{-1} = t_c/\tau$  is the width of the distribution of the capillary transit times inside a voxel,  $\gamma(a, z)$  is the Gamma function,  $E$  is the extraction fraction of CA that is extracted into the EES during a single capillary transit. The Ktrans and  $v_p$  parameters are not calculated directly from the fitting process as in ETM. Therefore, these parameters are determined using the relations:  $K_{trans} = FE$ ,  $v_p = (1 - Hct) * F t_c$  [9]. For our analysis hematocrit (Hct) value were considered 0.45 for male and 0.42 for female patients.

To assess the quality of the fits between the data and the pharmacokinetic models (assume  $G(x, t)$ ) the root mean squared error (RMSE) was chosen. Considering, parameters  $x = \{x_1, x_2, \dots, x_p\}$  and  $d$  data points of size  $N$  the RMSE formula is given by Eq. (4).

$$RMSE = \sqrt{\sum_{i=1}^N \frac{(G(x, t_i) - d_i)^2}{N}} \quad (4)$$

## 7. Correlation analysis

As a first step, perfusion derived maps were resized through cubic interpolation (to mitigate information loss) to match the size of the diffusion parametric maps. Then the slice location of each DICOM tag was used to align the two sequences in the z-axis. Images from each 4D dataset were masked according to the corresponding 3D ROI delineated by an experienced (> 30 years) musculoskeletal radiologist. To avoid false or biased results of correlation between non perfused areas

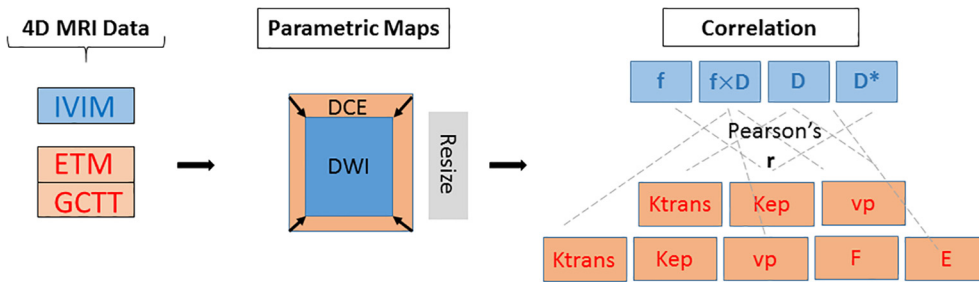


Fig. 2. Image post processing workflow (data acquisition, generation of parametric maps and resizing, Pearson’s correlation between derived markers).

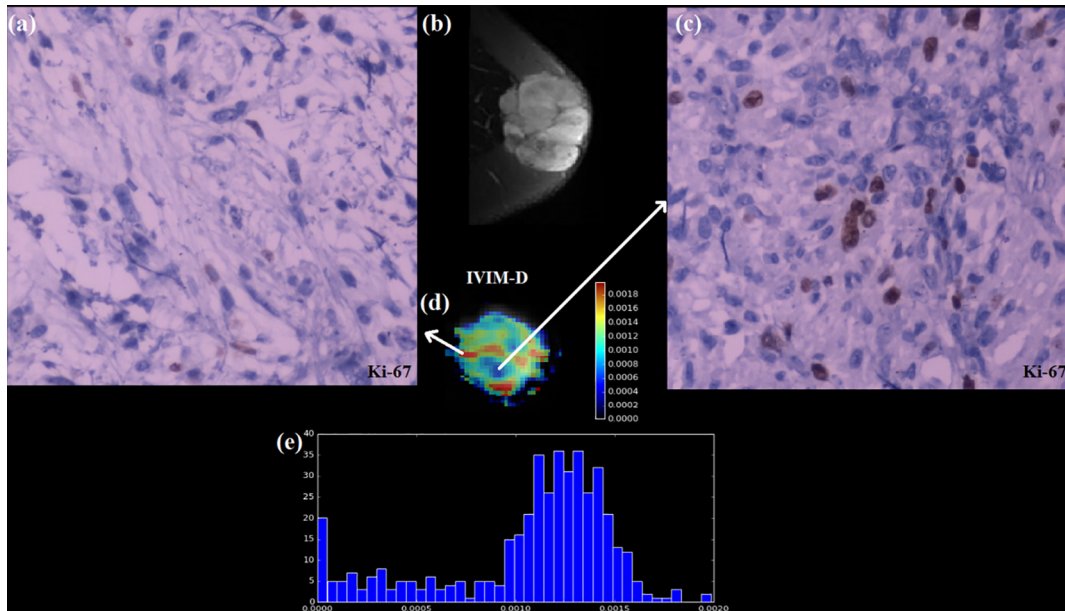


Fig. 3. Malignant tumor (MPNST) of the left shoulder (axial STIR MR image (b)). Histopathologic analysis Ki-67 ( $\times 100$ ) showed alternation of areas with low (a) and high (c) cellularity areas. Corresponding IVIM-D parametric map (d) and corresponding histogram (e).

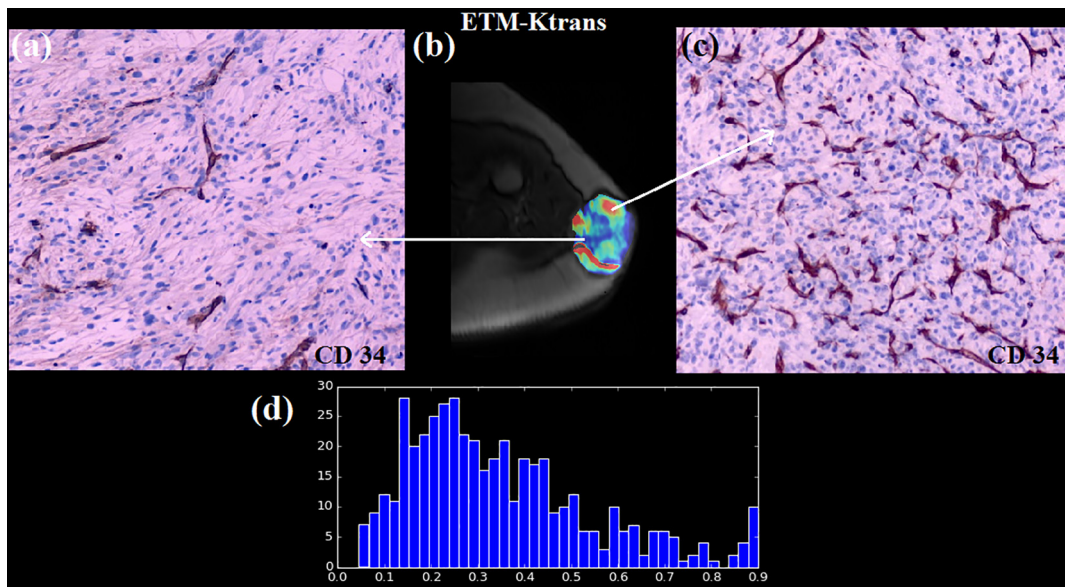


Fig. 4. Malignant tumor (MPNST) of the left shoulder. ETM Ktrans map is overlaid to T1 VIBE image for the tumor ROI (b). Histopathologic analysis CD34 ( $\times 100$ ) showed diverse pattern of vascularity (i.e. areas of low vascularity (a) neighboring to areas of high vascularity (c)). ETM Ktrans corresponding histogram (d).

**Table 1**

Pearson's correlation coefficient between DWI and DCE derived parametric maps and percentages of voxel overlap with high Ktrans and low ADC as described in materials and methods section.

Patients	Pearson's r		DCE–DWI overlap
	f–vp ETM	f–vp GCTT	%
p.1	0.310873	0.534515	23.509
p.2	0.181833	0.630569	6.009
p.3	0.149587	0.570498	24.493
p.4	0.24293	0.38424	28.62
p.5	0.608346	0.49826	14.537
p.6	0.413949	0.618321	6.898
p.7	0.019283	0.524793	30.208
p.8	0.30969	0.482717	20.439
p.9	0.468085	0.471851	8.698
p.10	0.208291	0.514515	31.344
p.11	0.168474	0.483627	28.808
p.12	0.46131	0.698278	11.772
p.13	0.050655	0.586594	18.39
p.14	0.485701	0.454904	10.838
p.15	0.41729	0.671383	6.681
p.16	0.600212	0.510584	9.756
p.17	0.164873	0.62538	9.597
p.18	0.417714	0.476529	10.998
p.19	0.224486	0.551787	15.431
p.20	0.311413	0.609723	6.241
p.21	0.166259	0.667271	27.567
p.22	0.340793	0.647787	28.619
p.23	0.205189	0.564165	17.271
p.24	0.361632	0.540817	17.231
p.25	0.375686	0.403571	13.442
mean	<b>0.306582</b>	<b>0.532072</b>	

( $vp < 0.05$  or  $f < 0.05$ ) were excluded from the analysis. Thus for every 3D ROI Pearson's correlation coefficient was calculated by (5).

$$r_{f, vp} = \frac{\sqrt{\sum_{i=1}^N (f_i - \bar{f})(vp_i - \bar{vp})}}{\sqrt{\sum_{i=1}^N (f_i - \bar{f})^2} \sqrt{\sum_{i=1}^N (vp_i - \bar{vp})^2}} \quad (5)$$

A graphical representation of the post processing process is shown in Fig. 2 describing the steps from data acquisition to the correlation of

all possible pairs of IVIM ( $f, D, D^*, f \times D, f \times D^*$ ) and DCE (Ktrans, Kep, vp, E, F) derived parameters.

## 8. Spatial identification of tumor aggressiveness

As both high cellularity and high vascular supply are markers of tumor aggressiveness, we calculated the percentage of tumor voxels meeting both criteria of low D and high Ktrans. Between the two models used for Ktrans extraction in this study we proceeded in this step with the ETM based calculation as it is more widely used and tested for quantitative studies [12]. For every 3D whole tumor ROI, the mean value of D and Ktrans were used as thresholds between high and low cellularity and vascularity respectively.

## 9. Results

The best aimed value describing tissue cellularity, is D calculated by the IVIM model deprived of the contribution of macro-diffusion movement (blood flow) from the vascular part of the tissue. Voxel based parametric maps were calculated for all patients and results were studied for reference based on the histopathologic analysis of the central tumor slice and more specifically Ki-67 stain images, showing nuclei density and mitotic activity and thus cellularity (Fig. 3). Similarly, CD 34 stain was used for assessing regional tumor vascularity (Fig. 4).

In terms of fitting accuracy, both pharmacokinetic models performed equally well, exhibiting low RMSE values. The mean RMSE and standard deviation values for ETM and GCTT models were  $RMSE_{ETM} = 0.0879 \pm 0.1264$  and  $RMSE_{GCTT} = 0.1062 \pm 0.1350$  respectively.

The Pearson's correlation r of both vp-ETM and vp-GCTT with f-IVIM per patient, as markers of tumor perfusion, is presented in Table 1. The third column of Table 1 summarizes the % percentage of volume overlap between voxels meeting both criteria of high cellularity (low D) and high vascular permeability (high Ktrans) as described in Correlation Analysis. The mean r values of the patient cohort are  $> 0.5$  ( $r > 0.5$ : linear relationship) only for f-IVIM and vp-GCTT. To graphically illustrate the linear relationship of f-IVIM and vp-GCTT quantile–quantile plots (q–q plots) were also appended in Fig. 5 for a

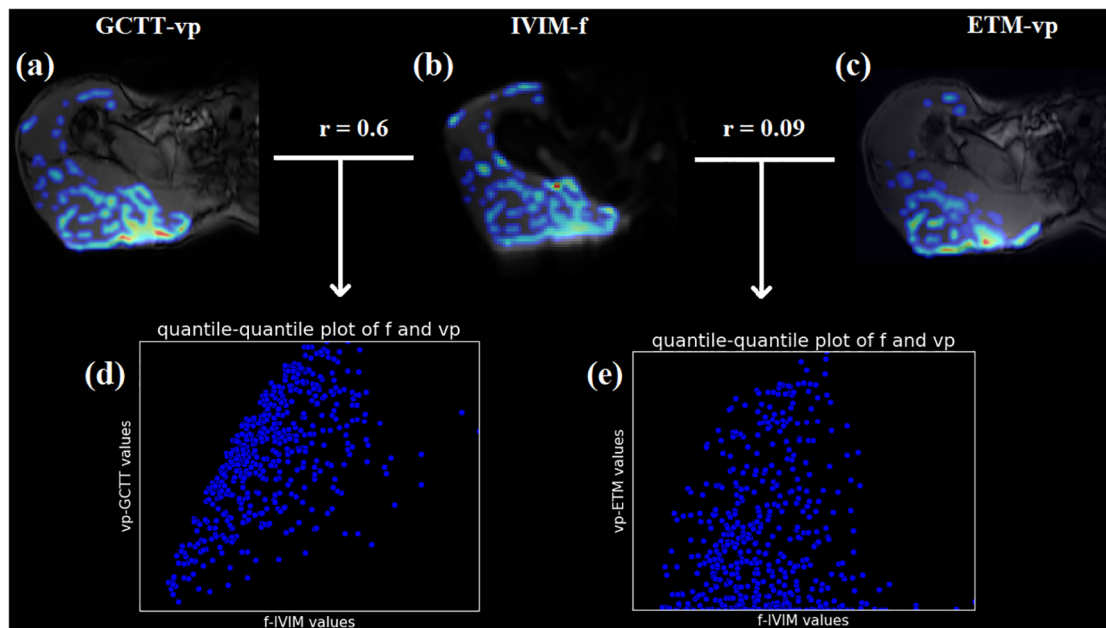


**Fig. 5.** Parametric vp maps for an Ewing sarcoma of the right shoulder computed by: GCTT (a) and ETM (c) models. In the middle IVIM-f parametric map. In the lower part, q–q plot between f and GCTT–vp (d) clearly shows the linear relationship with Pearson's  $r = 0.6$ , while q–q plot between f and vp ETM (e) shows neutral correlation (Pearson's  $r = 0.09$ ).

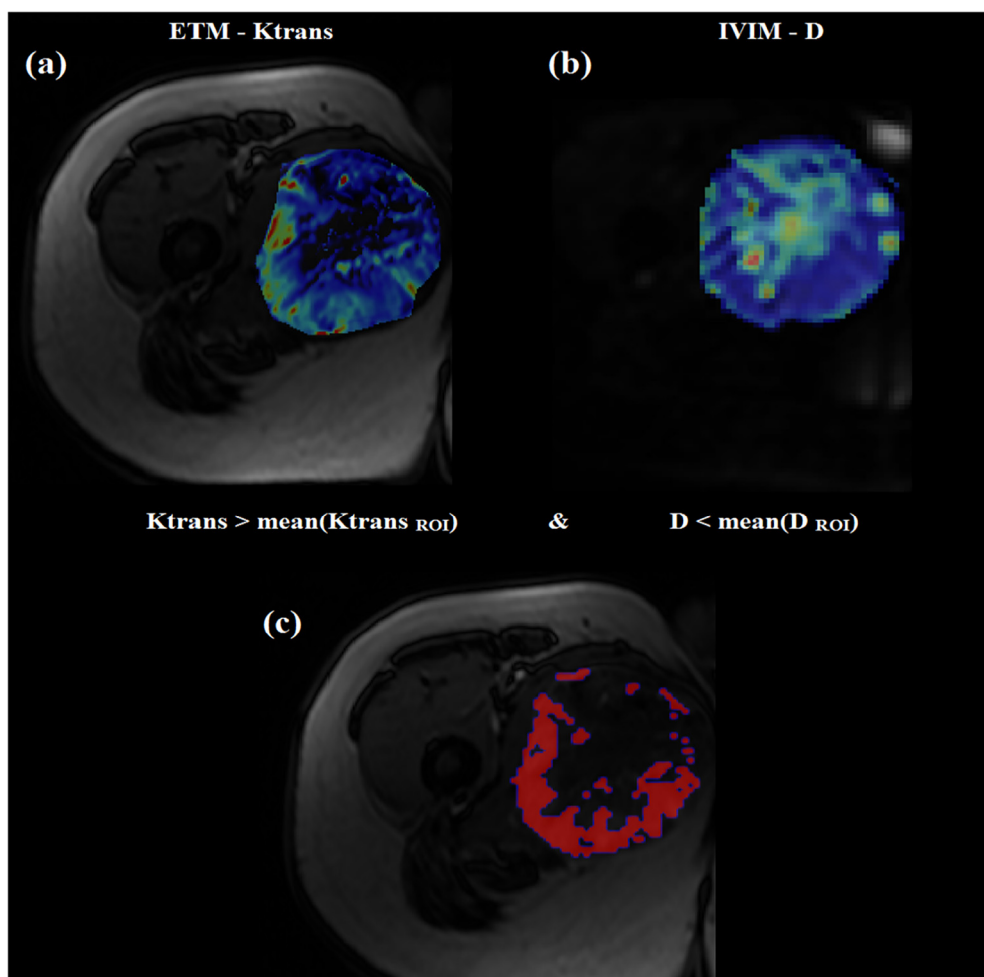


Fig. 6. Dedifferentiated liposarcoma of the right thigh. Parametric maps of ETM Ktrans (a) and IVIM D (b) superimposed on DCE T1 GE and DWI images respectively. The lower image (c) shows the areas meeting both criteria of high Ktrans (high vascular permeability) and low D (high cellularity).

patient with Ewing sarcoma of the shoulder. It is important to note that the corresponding p-values per patient were significantly lower than  $10^{-5}$  for all cases because the analysis was voxel based rather than ROI based.

As a next step we studied the spatial correlation of the most aggressive tumor areas as indicated by the two different MR methodologies, i.e. cellularity as indicated by D and tumor vascular supply as indicated by DCE Ktrans. A criterion of low D and high Ktrans was set and then the intersection of the two subsets of tumor voxels was graphically represented overlaid on anatomy to constitute a guide for tumor biopsy within such heterogeneous and large masses (Figs. 6 and 7).

## 10. Discussion

The first aim of the present study was to validate associations of IVIM derived parameters with known DCE models on STT data. Secondly, the most aggressive sub-regions of the tumor were located individually, as indicated either by DWI or DCE and then the spatial correlation between two methods was presented.

Initially we examined the sensitivity of IVIM to measure perfusion related parameters as this could theoretically simplify an MR oncologic protocol including both DWI and DCE sequences and also help to avoid the intravenous injection of contrast medium. This in turn positively affects acquisition time, patient discomfort and imaging cost whereas there are cases that gadolinium administration is clinically contraindicated. Relevant published studies have shown positive correlation

of DCE and DWI MRI parameters. Suo et al. performed semi-quantitative perfusion DCE analysis on breast cancer with a 3T MR scanner reported correlation of (f-IVIM) with relative enhancement ratio exhibiting  $r = 0.55$  and f-IVIM with AUC with  $r = 0.56$  [13]. In the brain region two correlative DWI-DSC studies by Kim et al. [14] and Federau et al. [15] reported correlation of f-IVIM and CBV with  $r = 0.67$  and  $r = 0.75$  respectively. The experimental DWI protocol of the latter consisted of 16b-values and this can partially explain the high r value reported. To the best of our knowledge this is the first DCE and DWI study concerning soft tissue sarcomas.

The results of the first part showed positive correlation between f-IVIM and vp-GCTT with a Pearson's  $r$  of 0.532 while the correlation between f-IVIM and vp-ETM was neutral,  $r = 0.306$ . It is important to note that our analysis sought correlation between all pairs of DWI ( $f, D, D^*, f \times D, f \times D^*$ ) and DCE (Ktrans, Kep, vp, E, F) derived parameters with r values ranging from  $-0.132$  to  $0.263$  indicating no significant correlation.

DCE derived parameter values and repeatability can vary widely by analytical methodology [16]. As this work deploys two different models for DCE data quantification differences between parametric maps calculated by GCTT or ETM models respectively are expected because of different assumptions made (number of compartments, directionality of CA transfer between the blood plasma and the EES). Indicatively Fig. 8 shows the differences between vp-GCTT and vp-ETM not only in the absolute values but also in the pattern of the parametric map. This variability is a possible explanation for the positive correlation between vp-GCTT and f-IVIM as opposed to the neutral correlation of vp-ETM

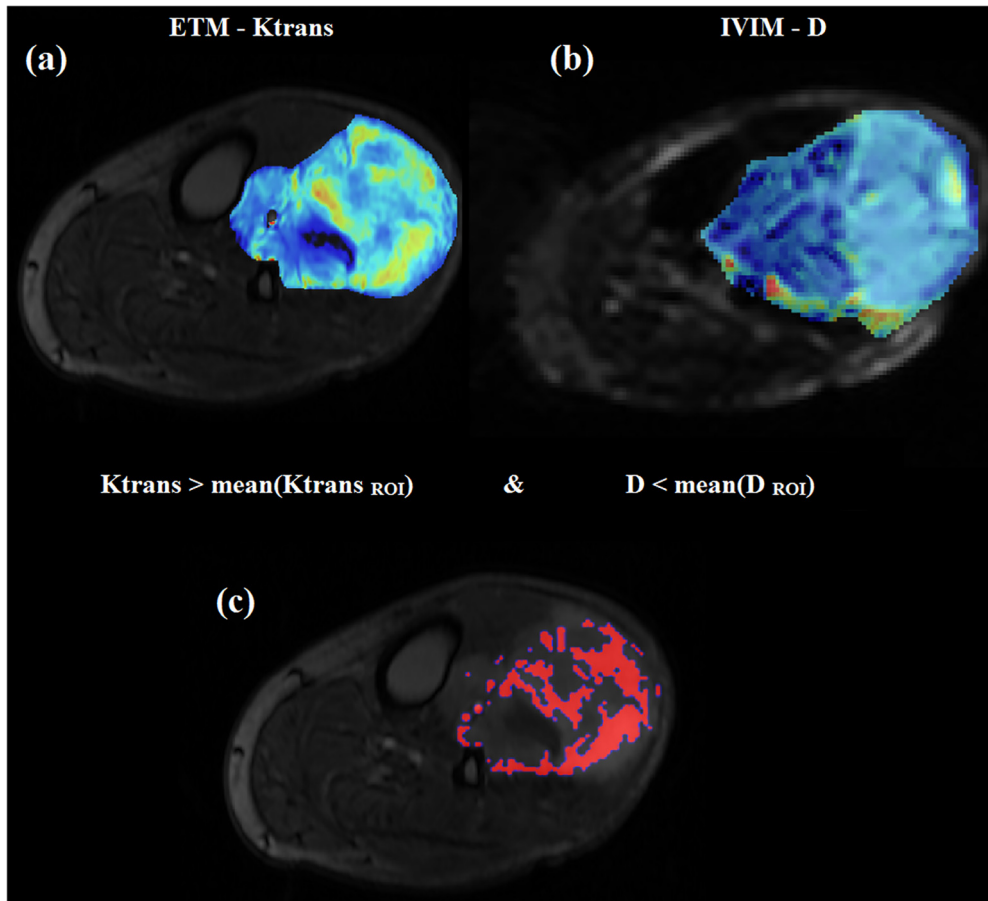


**Fig. 7.** Malignant tumor (MPNST) of the left calf. Parametric maps of ETM Ktrans (a) and IVIM D (b) superimposed on DCE T1 GE and DWI images respectively. The lower image (c) shows the areas meeting both criteria of high Ktrans (high vascular permeability) and low D (high cellularity).

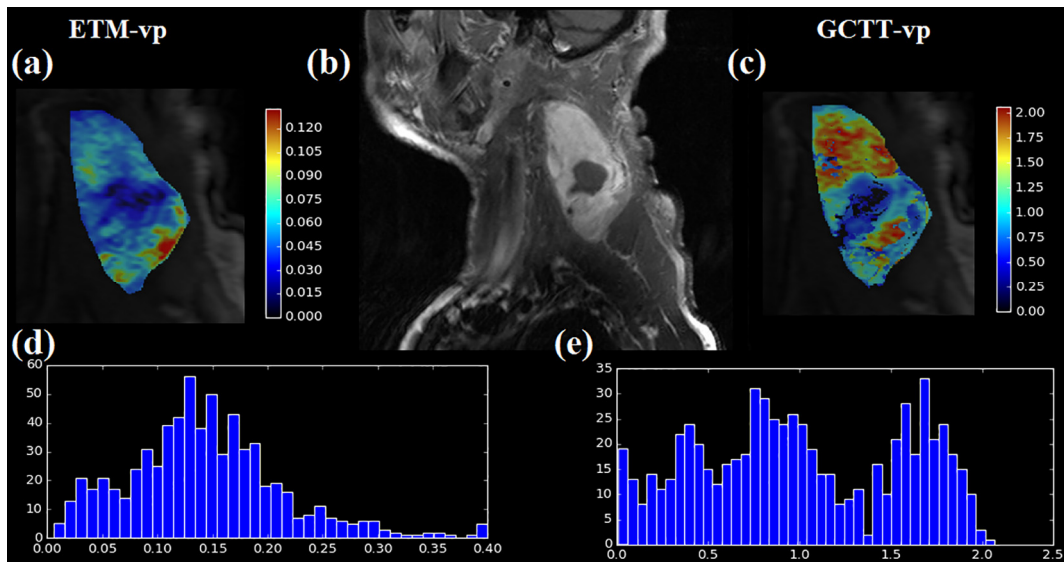


**Fig. 8.** Alveolar soft tissue sarcoma of the neck (same patient as in Fig. 1). (a) ETM vp map, (b) parasagittal fat suppressed contrast enhanced T1W MR image. (c) GCTT-vp map, (d) ETM vp histogram, (e) GCTT vp histogram.

and f-IVIM.

With regard to the second part of the analysis, we used the mean value of each biomarker for thresholding but the use of other histogram metrics, such as 5%, 10% percentiles, could have also been used for the same purpose. All patients had non-zero volume overlap between voxels with metrics showing aggressiveness indicated from the two

different methodologies. Preliminary results from this study previously reported [17], had shown spatial correlation on a smaller patient population. A frequently encountered finding among the patient cohort was the thresholded DCE-DWI overlap in the periphery of the tumor which was consistent with findings of histopathologic analysis. This in turn shows the possible application of DCE-DWI overlap for

preoperative biopsy guidance as in all cases overlapping voxels were not dispersed in the tumor 3D tumor volume but congregated in specific sub-regions as depicted with red in the lower part of Figs. 5 and 6.

The most challenging datasets proved to be in the abdominal region, probably due to respiratory artifacts hampering DCE-DWI alignment and degradation of 4D data quality. Another limitation of our study arises from the necessary step of resizing the DCE parametric maps to match the size of DWI maps. Among available interpolation methods, bicubic interpolation was preferred over linear or nearest neighbor as it outperforms the other two [18].

In conclusion, a free correlation study among all DCE and DWI derived pairs of parameters showed a linear relationship between  $f$ -IVIM and  $vp$ -GCTT in patients with soft tissue sarcomas. Moreover the spatial relationship between low cellularity and high vascular permeability areas was illustrated as a possible visual guide for pre-operative biopsy.

### Acknowledgements

This research is co-financed by Greece and the European Union (European Social Fund – ESF) through the Operational Programme «Human Resources Development, Education and Lifelong Learning 2014–2020» in the context of the project “Newer techniques in MR Imaging of musculoskeletal disorders” (MIS 5004349). The authors wish to acknowledge Professor *Thomas G. Maris* for MRI protocol optimization, Dr. *Eleni Lagoudaki* for the histopathologic analysis, Professor *Eelco De Bree* for performing surgical tumor excision, and Professor *Kostas Marias* for his support and guidance.

### References

- [1] Essig M, Shiroishi MS, Nguyen TB, Saake M, Provenzale JM, Enterline D, et al. Perfusion MRI: The Five Most Frequently Asked Technical Questions. *Am J Roentgenol* 2013;200(1):24–34. <https://doi.org/10.2214/AJR.12.9543>.
- [2] Tofts P. *Quantitative MRI of the Brain*. John Wiley & Sons Ltd; 2003.
- [3] Bihan Le, Denis Eric, Breton DL. Separation of Diffusion and Perfusion in Intravoxel Incoherent Motion MR Imaging. *Radiology* 1988;168:497–505.
- [4] WHO Classification of Soft Tissue Tumours 139 2006 35 39.
- [5] Lester SC. *Manual of surgical pathology*. Saunders/Elsevier 2010.
- [6] Kwee TC, Galbán CJ, Tsien C, Junck L, Sundgren PC, Ivancevic MK, et al. Comparison of apparent diffusion coefficients and distributed diffusion coefficients in high-grade gliomas. *J Magn Reson Imaging* 2010;31:531–7. <https://doi.org/10.1002/jmri.22070>.
- [7] Taheri S, Gasparovic C, Shah NJ, Rosenberg GA. Quantitative measurement of blood-brain barrier permeability in human using dynamic contrast-enhanced MRI with fast T1 mapping. *Magn Reson Med* 2011;65:1036–42. <https://doi.org/10.1002/mrm.22686>.
- [8] Tofts PS. Modeling tracer kinetics in dynamic Gd-DTPA MR imaging. *J Magn Reson Imaging* 1997;7:91–101.
- [9] Schabel MC. A unified impulse response model for DCE-MRI. *Magn Reson Med* 2012;68:1632–46. <https://doi.org/10.1002/mrm.24162>.
- [10] Lawrence Keith S St, Lee Ting-Yim. An adiabatic approximation to the tissue homogeneity model for water exchange in the brain: i. theoretical derivation. *J Cereb Blood Flow Metab* 1998;18(12):1365–77.
- [11] Brix G, Salehi Ravesh M, Zwick S, Griebel J, Delorme S, Brix G. On impulse response functions computed from dynamic contrast-enhanced image data by algebraic deconvolution and compartmental modeling. *Phys Medica* 2012;28:119–28. <https://doi.org/10.1016/j.ejmp.2011.03.004>.
- [12] Litjens GJS, Heisen M, Buurman J, ter Haar Romeny BM. Pharmacokinetic models in clinical practice: What model to use for DCE-MRI of the breast? 2010 IEEE Int. Symp. Biomed. Imaging From Nano to Macro. IEEE 2010:185–8. <https://doi.org/10.1109/ISBI.2010.5490382>.
- [13] Suo S, Lin N, Wang H, Zhang L, Wang R, Zhang S, et al. Intravoxel incoherent motion diffusion-weighted MR imaging of breast cancer at 3.0 tesla: Comparison of different curve-fitting methods. *J Magn Reson Imaging* 2015;42:362–70. <https://doi.org/10.1002/jmri.24799>.
- [14] Kim HS, Suh CH, Kim N, Choi C-G, Kim SJ. Histogram analysis of intravoxel incoherent motion for differentiating recurrent tumor from treatment effect in patients with glioblastoma: initial clinical experience. *AJNR Am J Neuroradiol* 2014;35:490–7. <https://doi.org/10.3174/ajnr.A3719>.
- [15] Federau C, O'Brien K, Meuli R, Hagmann P, Maeder P. Measuring brain perfusion with intravoxel incoherent motion (IVIM): Initial clinical experience. *J Magn Reson Imaging* 2014;39:624–32. <https://doi.org/10.1002/jmri.24195>.
- [16] Ng CS, Wei W, Bankson JA, Ravoori MK, Han L, Brammer DW, et al. Dependence of DCE-MRI biomarker values on analysis algorithm. e0130168 *PLoS ONE* 2015;10. <https://doi.org/10.1371/journal.pone.0130168>.
- [17] Nikiforaki K, Kalaitzakis G, Ioannidis G, Maris TG, Marias K, Karantanas A. [OA046] Visualizing sites of increased cellularity and high permeability in soft tissue sarcomas. *Phys Medica* 2018;52:19. <https://doi.org/10.1016/J.EJMP.2018.06.118>.
- [18] Pan M, Yang X, Tang J. Research on Interpolation Methods in Medical Image Processing. *J Med Syst* 2012;36:777–807. <https://doi.org/10.1007/s10916-010-9544-6>.